Structural and magnetic properties of an anisotropic M-type LaCo-substituted strontium hexaferrite

Muriel Tyrman, Alexandre Pasko, Olivier de La Barrière, Frédéric Mazaleyrat

EPJ manuscript No.
(will be inserted by the editor)

Structural and magnetic properties of an anisotropic M-type LaCo-substituted strontium hexaferrite.

Muriel Tyrman[12], Alexandre Pasko[1], Olivier De La Barrière[1] and Frédéric Mazaleyrat[1]

[1] SATIE, ENS Cachan, CNRS, Université Paris-Saclay, 61 av Président Wilson, F-94230 Cachan, France
[2] LISV, 10-12 av de l'Europe, F-78140 Vélizy, France

Received: date / Revised version: date

Abstract. Rare-earth-free permanent magnets returned to the forefront of scientific and technological concerns about the environmental and economical issues. The emergence of new markets, control of costs and availability of raw materials encourage to look for alternative materials containing much less, or no, rare earth elements selected from the most common and most available. The hexaferrite doped with lanthanum and cobalt present interesting properties to succeed the rare-earth magnets. The structural and magnetic properties of a strontium hexaferrite are presented in this paper, and two models are developed in order to correlate structural and magnetic properties.

1 Introduction

Permanent magnets, or hard magnetic materials, represent an important part for the automobile industry because they are many in electrical motors (currently, a car contains an average of thirty of those motors). This kind of magnet must have a high resistance to demagnetization, especially at high temperature. In the domain of magnets, no rare-earth-free material will have a coercivity as high as the $Nd_2Fe_{14}B$ and its partially Dy-substituted by-products, and especially as the $SmCo_5$, which has a much higher coercivity. However, in many applications, it is not necessary to have such powerful magnets. This is particularly true in the case of electrical machines for automotive drive for which new topologies and the dual excitation (coils and magnets) can reduce the amount and/or the performance of the magnets at a constant power density. Due to the distribution of mineral resources, and the near monopoly of one country on their refining, rare earth elements have become a major political and economical issue. Therefore, the question is : to what extent the industry is able to do without these elements? For the automotive industry, it is necessary to have magnets whose properties remain interesting when the temperature varies. Indeed, the electrical motor of a vehicle can reach 200°C in a car staying under the sun, and we know that magnets containing rare earth elements have a decreasing coercive field, H_c, with increasing temperature, unlike hexagonal ferrites where H_c increases with temperature. Furthermore, hexaferrites are inexpensive and easy to manufacture ($< 5\,\$kg^{-1}$), unlike rare earth magnets ($> 100\,\$kg^{-1}$). Presently, the use of a less efficient than NdFeB magnet means using a ferrite magnet with a magnetization three times lower and with an energy density significantly ten times smaller. So researchers and manufacturers need urgently to answer two questions, to improve the performance of ferrite magnets and to look for magnets with intermediate performances between standard ferrite and rare earth magnets[1]. In the early 2000s, it had been demonstrated that the partial lanthanum to strontium and cobalt to iron substitutions increase significantly the coercivity ([2],[3] and [4]) and the remanence of hexaferrites. On the other hand, the grain size reduction can also increase the coercivity by nearly a factor 2 if the grain size is less than 100 nm [5]. However such a grain size reduction makes the grains single-domain, which produce strong dipolar forces opposed to the orientation of the magnetic particles under a magnetic field. Because it is difficult to produce anisotropic magnets from single-domain magnetic particles, it is necessary to find a compromise ensuring a proper orientation and an optimization of the coercive field. To this end, we investigated the magnetic properties of an anisotropic strontium hexaferrite, with the chemical composition $(Sr, La)(Fe, Co)_{12}O_{19}$.

2 Experimental procedure

The magnet studied here was provided in the form of a $30 \times 10 \times 5\text{mm}^3$ rectangular prism. The chemical and structural analysis was performed by a Hitachi S-3400N VP scanning electron microscope (SEM), in image and in chemical analysis (EDX) modes.

The SEM images were performed on the fractured edge of a magnet and the chemical analysis on the face parallel to the easy axis. The XRD analysis was made by means of a X'Pert pro diffractometer in $\theta - 2\theta$ geometry using a Co-source in the angular range $15 < 2\theta < 90°$ with a step of 0.02°. Two spectra were recorded, one in the plane parallel to the easy axis and the other in a perpendicular

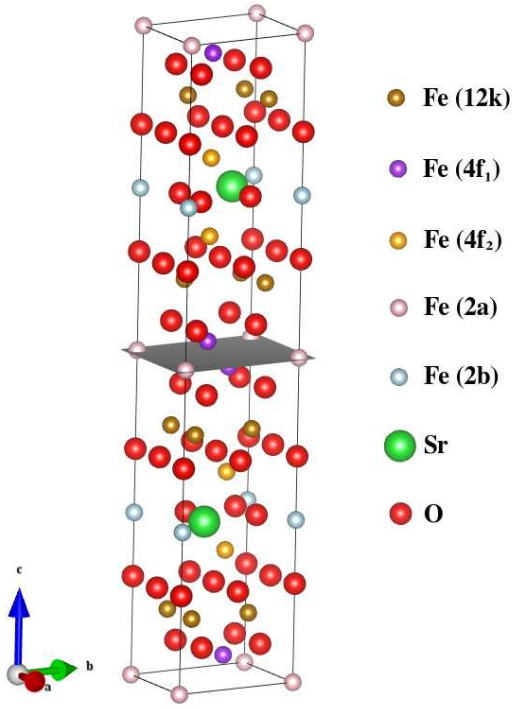

Fig. 1. Crystallographic lattice of strontium hexaferrite.

Table 1. Chemical composition determination(SEM).

Element	% atomic	% error	molar conc.
Sr	2.38	10.08	0.75
O	59.27	8.58	18.78
La	0.48	20.99	0.15
Fe	36.91	1.41	11.70
Co	0.96	14.95	0.30

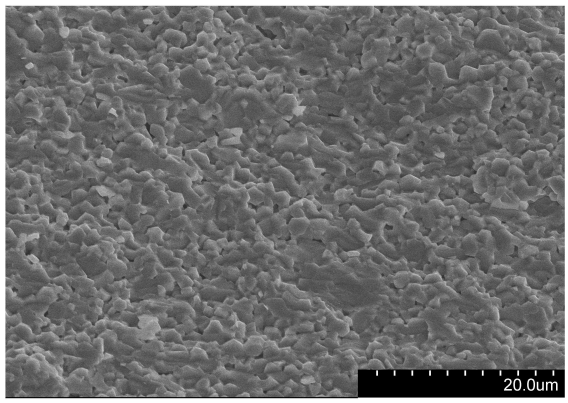

Fig. 2. SEM image of the strontium hexaferrite (1).

plane. They have been analysed using the Rietveld based freeware Maud version 2.33, using the texture option, with a Gaussian model.

The magnetic properties of our sample were determined by means of a vibrating sample magnetometer (LakeShore VSM). A 2 mm cube was prepared, carved into a commercial magnet. The first hysteresis loops were performed at room temperature (T=294 K). In order to observe the anisotropic properties experimentally, we plotted hysteresis loops for different values of the angle between the easy axis and the applied field:0°, 45° and 90°.

The first order reversal curves (FORC) were measured in the easy magnetization axis starting from +1.4 T. The reversal points were chosen by selecting the applied fields corresponding to the points of the descending branch of the major loop, in order to scan the loop in the most homogeneous manner. The reversal curves were measured from the reversal point to +1.4 T again.

The measurements at high temperatures were carried out under argon flow from room temperature (294 K) to 523 K with a step of 50 K.

3 Micro-structural properties of the strontium hexaferrite

The strontium hexaferrite is M-type, in other words the crystallographic structure is the hexagonal structure of the magnetoplumbite (fig.1). In simple Sr (or Ba) hexaferrite, because the magnetic carriers are only the zero orbital momentum Fe^{3+} ions, the anisotropy has a purely structural origin: all magnetic momenta are directed parallel (2a, 2b, 12k sites) or anti-parallel ($4f_1$ and $4f_2$ sites) to c-axis. Co^{2+} substitution to Fe^{3+} increases the magnetocrystalline anisotropy together with a reduction of the total magnetization limited by the distribution of Co cations in parallel (2a) and antiparallel sub-networks ($4f_2$ after [2]). La^{3+} is substituted to Sr^{2+} to ensure the electroneutrality thanks to its comparable ionic radius.

The chemical analysis by SEM gives the proportions of the elements in the sample (table 1). Considering the accuracy of the technique, the chemical formula is estimated to be $Sr_{0.8}La_{0.2}Co_{0.3}Fe_{11.7}O_{19}$ as the heavy element to transition metal content must be 1/12. It is however slightly off-stoichiometric since La doesn't compensate Co completely, but a 1% lack of electrons in 2p orbitals of oxygen is always acceptable. Also it cannot be excluded that a part of Co ions are in the 3+ state.

The SEM images with a magnification of ×2000 (fig.2) clearly shows the fine and homogeneous structure of the magnet free of pores and cracks on the fractured face. Higher magnification (×5000 in fig.3) allowed to determine an average size of particles $D_{SEM} = 1.5\,\mu$m with $0.35\,\mu$m standard deviation.

The XRD spectra are represented on fig.4. The pattern noted easy axis was recorded using the face normal to easy axis as reflexion surface. Indexation of peaks shows that the stronger reflections correspond to (00l) planes which are parallel to c-axis. The nearly total extinction of all other peaks clearly shows the strong structural anisotropy of the ceramic. The only other relevant peak on the right of (008) corresponds to (107) which shows that there is a narrow distribution of c-axes around the main direc-

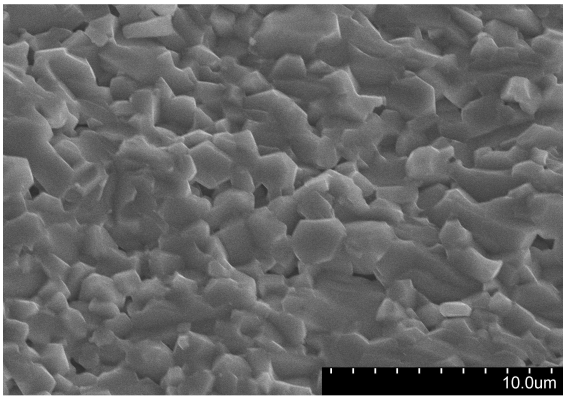

Fig. 3. SEM image of the strontium hexaferrite (2).

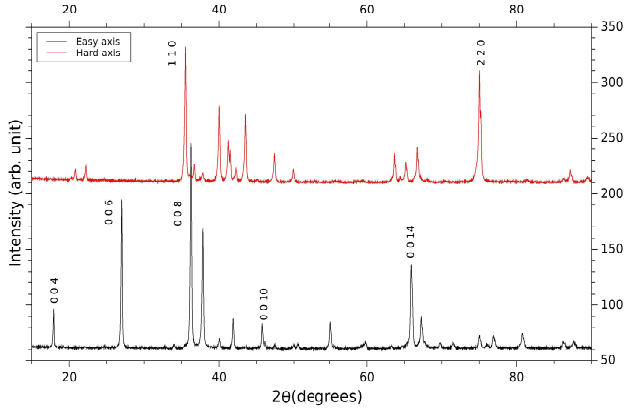

Fig. 4. XRD spectra in function of the sample orientation : easy axis or hard axis.

tion. If the spectrum is recorded using a surface parallel to the easy axis of the magnet as incident plane (upper pattern on fig. 4), mainly (110) and (220) reflexions planes appear which naturally correspond to the lateral faces of the hexagonal prism, showing again the strong texture. Rietveld refinement has been conducted simultaneously with the two patterns and introducing the texture in the form of a Gaussian distribution centered on $\langle 00\ell \rangle$ axis. The fitting yields the lattice parameters $a = 0.58822\,\text{nm}$, $c = 2.30490\,\text{nm}$, and the full width half maximum of the Gaussian distribution FWHM=34°. The expected parameters for an undoped SrM hexaferrite are in the same range of values : $a = 0.58844\,\text{nm}$, $c = 2.30632\,\text{nm}$ [6]. From the lattice parameters a and c, we can determine the angle ϕ between the plans (008) and (107) which is $\phi \approx 33°$. From the XRD spectra, the crystallite size $D_{XRD} = 174\,\text{nm}$. This value is much smaller than that observed by SEM which actually shows agglomerates of particles.

4 Determination of the texture from magnetic measurements

According to the Stoner and Wohlfarth [7] model, we assume that our material is a set of spherical non interacting

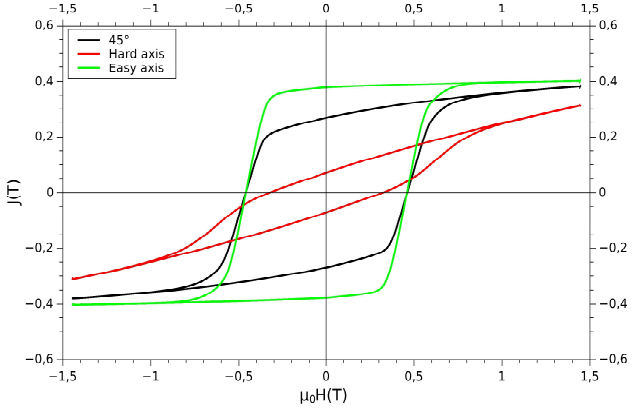

Fig. 5. Strontium hexaferrite hysteresis loops as a function of the orientation of the sample.

single-domain particles (thus there is no shape anisotropy), with a development of the uniaxial anisotropy limited at second order (equation 1, and $K_1 \gg K_2$). The easy axis of magnetization is oriented along the c-axis of the particle. To determine the anisotropy field H_k, the applied field needs to be perpendicular to the easy axis of the magnet. The energy equation for one particle is the sum of the magnetocrystalline and Zeeman energies :

$$E = K_1 sin^2(\theta) - HM_s cos(\alpha - \theta) \qquad (1)$$

If the field is exactly perpendicular to the c-axis, it is well known that the magnetization will be linear up to saturation and with no hysteresis. However, this condition is only met in single crystals. In other cases, it is possible to compute the hysteresis loop by numerical simulation using an algorithm to determine the local energy minima for a given angle α as described hereafter. If we simulate the major hysteresis loop, the initial magnetic state of the particle is known because it is saturated in the direction of H (the initial field is chosen higher than the expected anisotropy field). In this case, the initial energy state in known because eq.1 has a single minimum. The next state is determined from the last energy state known by choosing the nearest local minimum.

4.1 Uniform model

For the uniform model, we consider the material perfectly anisotropic and all particles have the same tilt angle ϕ with reference to easy magnetization axis. A basic outcome Stoner and Wohlfarth model [7] is that the remanence is the cosine of the angle (α) between the orientation of the applied field and the easy axis of magnetization of the crystal.

$$J_R = J_S cos\alpha \qquad (2)$$

From fig.5, the eq.2 allows to determine this angle depending on the position of the magnet relative to its easy axis (EA), see fig.6.

When the applied field is perpendicular to the EA of the magnet, the expected zero remanence and coercivity is not found. From the loop measured in the hard axis, the remanence indicates an angle $\alpha = 80°$ which corresponds to a tilt angle $\phi = \frac{\pi}{2} - \alpha = 10°$.

When the field is applied at 45° from the EA, $\alpha = 48°$ which confirms the misorientation. When studying hard magnets (especially NdFeB), it often happens that the magnetometer can't produce a field larger than H_k, so it's impossible to reach the saturation within the hard axis. In the present case the VSM used can't exceed 2 T. Therefore, a fitted demagnetization branch of the experimental hysteresis loop using the uniform model (fig.7) will allow in principle to determine H_k with a lower field. In this case, we have two fitting parameters, ϕ and H_k. The result is shown in fig.7, the anisotropy field is $\mu_0 H_k$=2 T and the tilt angle is $\phi = 10°$. It is noticeable that the present strontium hexaferrite has a higher anisotropy field compared to simple Sr-hexaferrite (1.7 T after [7]). The second order anisotropy constant can be determined from fig.6 as follows:

$$K_1 = J_S H_k / 2 \tag{3}$$

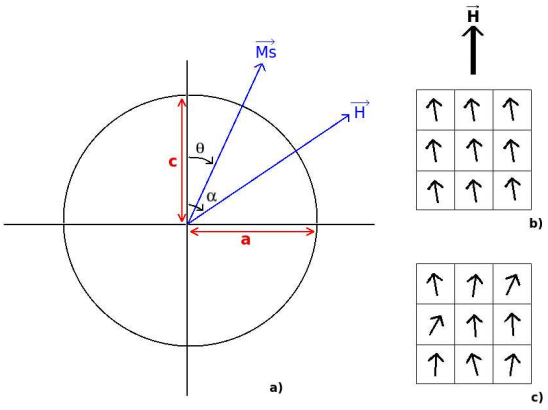

Fig. 6. a)Spherical magnetic particle, with c = a, c-axis = easy axis, b) ideal case : uniform misorientation, c) real case : statistic misorientation.

Therefore, considering a uniform misorientation of the present magnet, we end up with the anisotropy constant $K_1 \approx 3.10^5\, J.m^{-3}$.

Because the fitting with the uniform model is not very good in the high field region, and because the hypothesis is not much realistic, this result must be considered with a limited confidence.

4.2 Statistic model

We are interested here in a more realistic case, where the tilt angle will be distributed around the EA of the magnet. Based on the results for one particle, it is possible to create a distribution of particles with different angles α for a given field. An hysteresis loop can be computed for each angle and a sum of all other directions can be done affecting a statistical weight to each direction.

In order to determine the anisotropy constant, we are particularly interested here in the case where the magnetic field is applied along the hard axis of the magnet. We used a distribution of particles orientations with angles α between 0° and 90°, as a Gaussian centered on the EA (eq.4 with α our expectation and σ the standard deviation).

$$f(x) = \frac{1}{\sigma\sqrt{2\pi}} e^{-\frac{(x-\alpha)^2}{2\sigma^2}} \tag{4}$$

It is justified here to introduce a zero mean tilt angle because the EA axis of the magnet is determined by the applied field to the green powder during the orientation process. The best fit of the demagnetization branch of the loop is obtained by varying two parameters, H_k and σ. It is clearly observed in fig.7 that the fit is almost perfect from $+H_{max}$ to $-H_c$. We got $\sigma = 13°$ for an anisotropy field of $\mu_0 H_k$=1.97 T. Compared to the uniform model, the determination of the anisotropy constant is not significantly changed, but the degree of confidence is much higher. Most interesting is the value of σ. Indeed, in the sect.3, the XRD refinement gave a characterization of the texture also using a Gaussian distribution. Maud's output value is the FWHM = 34°, which is linked to the standard deviation by the relation FWHM=2.35*σ. So we finally get $\sigma = 14°$ from XRD. This result shows that the Stoner-Wholfarth fitting of the perpendicular loop is efficient, reliable and that it could be used to characterize the texture of the sample without XRD analysis. This result also confirms that the hypothesis $K_1 \gg K_2$ was perfectly justified at this temperature.

Looking the hysteresis loop (fig.7), it is observed that the ascending branch of the loop is not reproduced correctly above $+H_c$. In particular, the theoretical switching field is much higher than the experimental one (for perpendicular loops it is useful to distinguish the switching field from the coercive field because the value is the same for both only when the applied field is less than 45° from the easy axis EA). This effect is often called Brown's paradox and finds its origin in dipolar and exchange interactions between the grains. One could adapt Kronmüller formula eq.5, to describe this result :

$$H_s^{exp} = \alpha_{k_r} H_k - N_{eff} M_s \tag{5}$$

where α_{k_r} is a coefficient depending on the easy axis distribution – so actually H_k is the theoretical switching field – and N_{eff} an empirical factor reflecting the dipolar interactions and/or wall formation [8]. However, this approach is limited in terms of physical meaning and relation with the microstructure.

5 First order reversal curves and Preisach model

The Preisach model is generally used to simulate the hysteresis for soft magnetic materials. It is used here as a

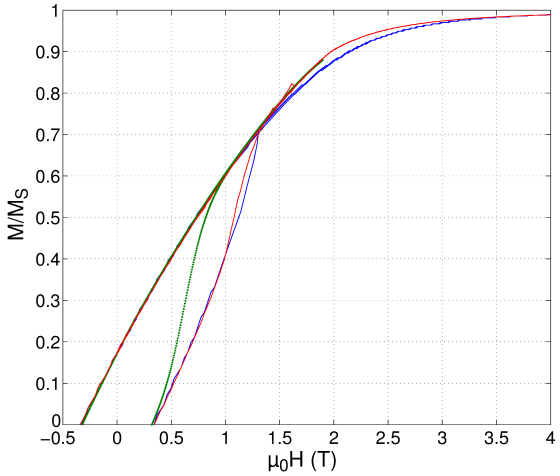

Fig. 7. Green curve: experimental hysteresis loop at room temperature, with the applied field along the hard axis; red curve: simulation of 30 particles distributed as a Gaussian centered on α=86°, with 13° the standard deviation; blue curve: simulation of one particle oriented in the direction α=80°(uniform model)

tool to characterise magnets, in other words it is used to characterise the magnetization process and the interactions within the material. Traditionally, minor hysteresis loops are used to determine the field distribution for this model. However, the minor loops recording needs a good demagnetization. Yet, for magnets, the magnetic demagnetization doesn't enable to reach the true demagnetised state. Since the thermal demagnetization is laborious, it is generally better to use first order reversal curves (fig.8), as proposed originally by Cornejo and Bertotti [9]. Those curves then allow us to study a distribution of coercive and interaction fields.

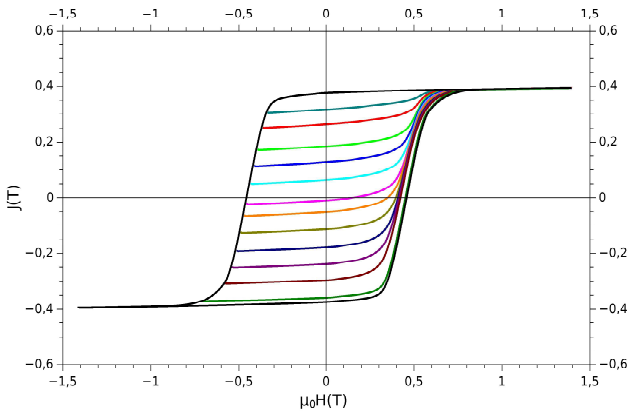

Fig. 8. First order reversal curves

Classically, Mayergoys [10] characterize the hysteron $M = f(H)$ by his positive and negative switching fields, H_α and H_β respectively. Very often for the magnets, authors prefer to plot the distributions of coercivity fields H_c and interaction fields H_i [8], as illustrated on the fig.9, defined by the eq.6 and eq.7:

$$H_c = (H_\alpha - H_\beta)/2 \tag{6}$$

$$H_i = (H_\alpha + H_\beta)/2 \tag{7}$$

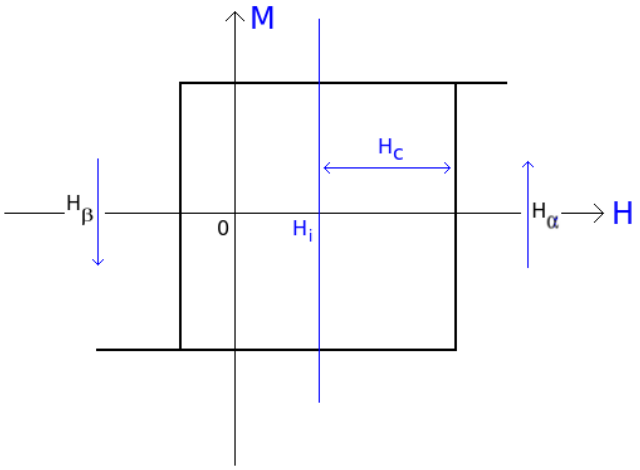

Fig. 9. Example of hysteron.

From the hysterons and the reversal curves, it is possible to determine an input function and an output function according to the eq.8 with x(t) = H(t) the input function and y(t) = J(t) the output function. The distribution function $\mu(H_\alpha, H_\beta)$ is based on the experimental measurements, while the function $\gamma_{H_\alpha,H_\beta}$ is linked to the characteristics of one elementary hysteron.

$$y(t) = \int\int_{H_\alpha \geq H_\beta} \mu(H_\alpha, H_\beta)\gamma_{H_\alpha,H_\beta} x(t)\, \mathrm{d}H_\alpha dH_\beta \tag{8}$$

However, it is also possible to use the eq.9 where the Everett function $E(H_\alpha, H_\beta)$ appears. This function is linked to the distribution function by a double integral (eq.10), which makes computations easier. Therefore, the eq.9 was used to characterize our material.

$$y(t) = -E(H_{\alpha_0}, H_{\beta_1}) + 2\sum_{k=1}^{n}[E(H_{\alpha_k}, H_{\beta_k}) - E(H_{\alpha_k}, H_{\beta_{k+1}})] \tag{9}$$

$$\mu(H_\alpha, H_\beta) = -\frac{\partial^2 E(H_\alpha, H_\beta)}{\partial H_\alpha \partial H_\beta} \tag{10}$$

The distribution function as a function of the interaction and coercive fields determined from the experimental measurements are plotted in the Preisach plane. When the magnetic material is hard, "T" shape distribution in the plane (H_c, H_i)[11] is expected.

For the present magnet, the Everett function obtained from the reversal curves is plotted on fig.10. The distribution function is then deduced from the Everett function and plotted in a Preisach plane as a function of $\mu_0 H_i$ and $\mu_0 H_c$ (fig.11) which is more appropriate for the study of the magnetization mechanisms.

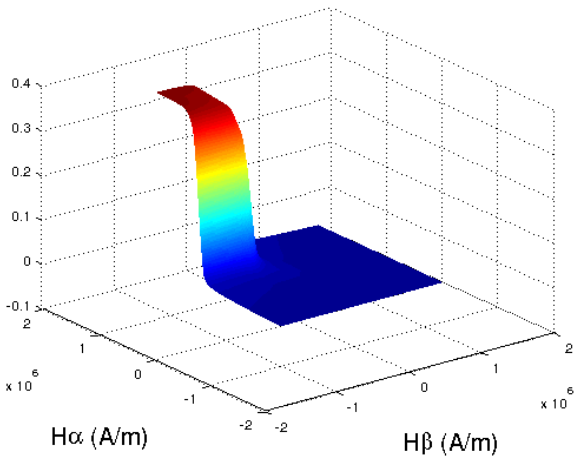

Fig. 10. Everett function $E(H_\alpha, H_\beta)$.

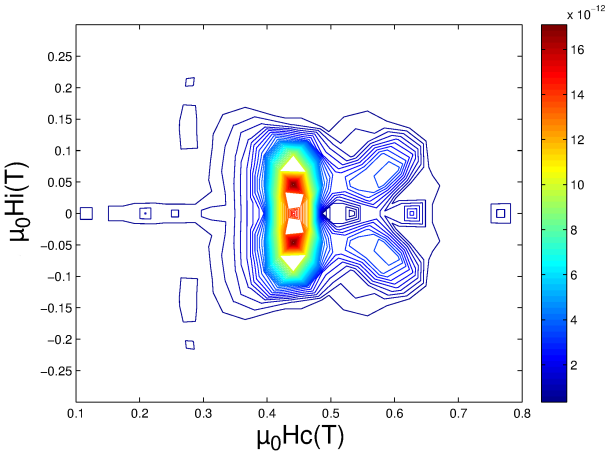

Fig. 11. Distribution function in the ($\mu_0 H_c$,$\mu_0 H_i$) Preisach plane.

The distribution obtained is perfectly symmetrical with respect to the $\mu_0 H_c$ axis, which indicates that the maximum applied field enables to saturate the material perfectly. The Preisach distribution is rather distributed along $\mu_0 H_i$ axis and reveals a relatively flat top with two maxima for a value of the coercive field of 0.44 T and an interaction field of $\pm$ 46 mT. The distribution of $\mu_0 H_i$ is narrow, as we can expect for a well oriented material. This figure is characteristic of a coercivity mechanics dominated by nucleation of the domain walls.

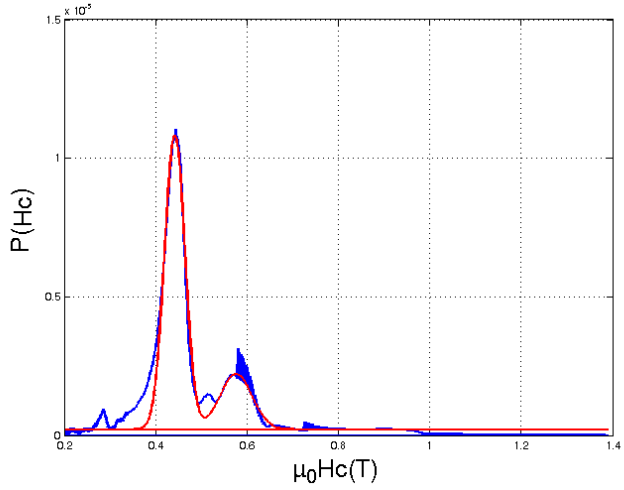

Fig. 12. Distribution function for $\mu_0 H_i$=0 T and $\mu_0 H_i$=0.046 T.

To study the magnetization mechanisms of the sample more easily, the distribution function is integrated for each value of H_i upon the values of H_c (fig.12). We obtain the distribution of the coercivity fields which, according Bertotti [8], can be fitted by Gaussian distributions. The first one is centered on $\mu_0 H_c$=0.44 T and has a standard deviation of only 22 mT. As the distribution narrower along H_c compared to its extension along H_i it may be attributed to nucleation of domain walls. The second Gaussian is centered on 0.58 T with a standard deviation of 35 mT, it can be attributed to either a second nucleation field or a pinning mechanism. It is remarkable that the reversal curves ascending from a reversal point $\mu_0 H > -0.58$ T don't reach the ascending branch of the major loop (fig.8). When the reversal point is chosen below this limit, the switching field of the reversal curve joints the major loop. The ratio between the area of the second Gaussian and the total area represent about a quarter of the distribution, which indicates that the domain walls nucleation governs the mechanism of magnetization in our sample. The major loop is reached for an applied field higher than 0.65 T, so practically this field is sufficient to fully magnetize this material.

6 Magnetic properties as a function of temperature

Finally, this work is completed by the study of hysteresis loops versus temperature in the range of interest for automobile applications. As shown in the fig.13, the remanence and the saturation decrease linearly when the temperature increases. In contrast, the rate of rectangularity J_R/J_S is independent of the temperature because it depends only of the orientation of the grains. The coercive field of the magnet increases appreciably, then it stabilises between 150°C and 250°C ($\mu_0 H_c$ = 0.56 T), and above it is expected to decrease up to the Curie temperature. This characteristic

of the hexaferrites (by opposition to rare-earth magnets) saves it from demagnetization at high temperature. From 373 K (100°C), the magnet behaves as an ideal magnet : $\mu_0 H_c > J_R$ and the second quadrant characteristic is perfectly linear (see fig.14). However, the maximum energy product $(BH)_{max}$ decreases by a factor 2 in the range of temperature referred (from 20 to 250°C) because the remanence decreases. Nevertheless, this feature has the advantage of thermal reversibility. By opposition to Nd-FeB magnets, when cooled after heating, there is no loss of magnetization, so an electrical machine can recover its full torque at room temperature even after heating to 250°C.

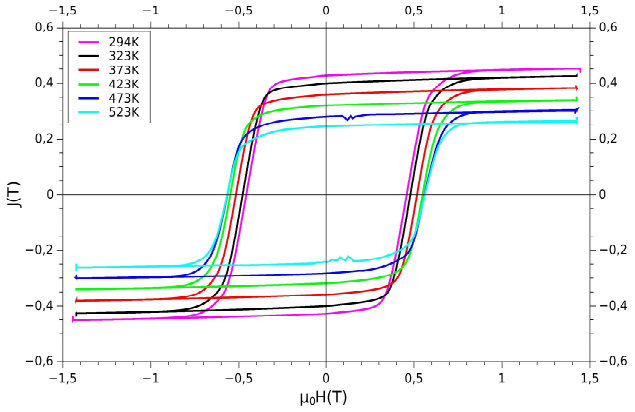

Fig. 13. Strontium hexaferrite hysteresis loops at different temperatures.

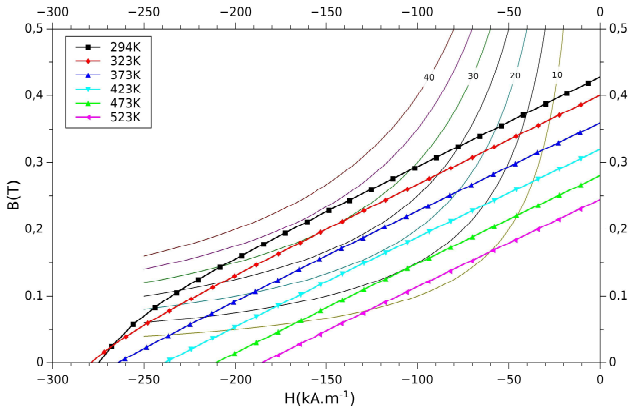

Fig. 14. Demagnetization curves, the lines are the (BH)=constant curves (kJ.m^{-3}). Over 323 K (50°C), the coercivity field in the B(H) plan is $\mu_0 H_{c_B} = J_R$.

7 Conclusion

This work allows the evaluation of the functional properties of this new generation hexaferrite hard magnets and to show the good performance regarding the demagnetization at high temperature, even if the energy product stays low compared to the rare-earth magnets. We have also precisely determined by several methods the degree of residual misorientation and its influence on the material properties, as well as the interactions in the material.

References

1. J.M.D. Coey, Scripta Materialia **67**, 524 (2012)
2. J.M. Le Breton, A. Morel, P. Tenaud, *Une nouvelle génération d'aimants permanents hexaferrites* (Ed. Techniques Ingénieur, Saint-Denis, 2005)
3. G. Wiesinger, M. Müller, R. Grössinger, M. Pieper, A. Morel, F. Kools, P. Tenaud, J.M. Le Breton, J. Kreisel, Phys. Status Solidi A **189**, 499 (2002)
4. A. Morel, J.M. Le Breton, J. Kreisel, G. Wiesinger, F. Kools, P. Tenaud, J. Magn. Magn. Mater. **242-245**, 1405 (2002)
5. F. Mazaleyrat, A. Pasko, A. Bartok, M. Lobue, J. Appl. Phys, **109**, 07A708 (2011)
6. R.C. Pullar, Prog. Mater. Sci. **57**, 1191 (2012)
7. B.D. Cullity, C.D. Graham, *Introduction to Magnetic Materials*, 2nd edn. (John Wiley & Sons, Hoboken, 2009)
8. G. Bertotti, *Hysteresis in Magnetism* (Academic Press, San Diego, 1998)
9. D.R. Cornejo, M. LoBue, V. Basso, G. Bertotti, F.P. Missell, J. Appl. Phys. **81**, 5588 (1997)
10. I.D. Mayergoyz, IEEE Trans. Magn. **22**, 603 (1986)
11. C.I. Dobrotă, A. Stancu, J. Appl. Phys. **113**, 043928 (2013)
12. R. Skomski, J.M.D. Coey, *Permanent Magnetism* (Taylor & Francis Group, New York, 1999)